

# Large-scale bias in the Universe II: redshift space bispectrum

L. Verde<sup>1</sup>, A.F. Heavens<sup>1</sup>, S. Matarrese<sup>2</sup>, L. Moscardini<sup>3</sup>

<sup>1</sup> *Institute for Astronomy, University of Edinburgh, Royal Observatory, Blackford Hill, Edinburgh EH9 3HJ, United Kingdom*

<sup>2</sup> *Dipartimento di Fisica Galileo Galilei, Università di Padova, via Marzolo 8, I-35131 Padova, Italy*

<sup>3</sup> *Dipartimento di Astronomia, Università di Padova, vicolo dell'Osservatorio 5, I-35122 Padova, Italy*

30 January 2018

## ABSTRACT

The determination of the density parameter  $\Omega_0$  from the large-scale distribution of galaxies is one of the major goals of modern cosmology. However, if galaxies are biased tracers of the underlying mass distribution, linear perturbation theory leads to a degeneracy between  $\Omega_0$  and the linear bias parameter  $b$ , and the density parameter cannot be estimated. In Matarrese, Verde & Heavens (1997) we developed a method based on second-order perturbation theory to use the bispectrum to lift this degeneracy by measuring the bias parameter in an  $\Omega_0$ -independent way. The formalism was developed assuming that one has perfect information on the positions of galaxies in three dimensions. In galaxy redshift surveys, the three-dimensional information is imperfect, because of the contaminating effects of peculiar velocities, and the resulting clustering pattern in redshift space is distorted. In this paper, we combine second-order perturbation theory with a model for collapsed, virialised structures, to extend the method to redshift space, and demonstrate that the method should be successful in determining with reasonable accuracy the bias parameter from state-of-the-art surveys such as the Anglo-Australian 2 degree field survey and the Sloan digital sky survey.

**Key words:** cosmology: theory - galaxies: clustering and redshift - galaxies: bias - large-scale structure of Universe

## 1 INTRODUCTION

One of the most important challenges of observational cosmology today is to measure the density parameter  $\Omega_0$ , that plays a key role in the determination of the properties and the geometry of the Universe. Geometrical tests such as number counts or the apparent magnitude as a function of the redshift of standard candles suffer from serious uncertainties, being sensitive to possible luminosity evolution with redshift and to the effect of a possible cosmological constant. This motivates attempting to measure  $\Omega_0$  in the local Universe from large-scale structure (LSS). Indeed, the only strong suggestions that the Universe may be close to the critical density comes from peculiar velocities or redshift distortions studies of LSS. These studies have the advantage that evolution and geometrical effects are negligible, but have some drawbacks. The amplitude of the distortions on linear scales allows measurement of the density parameter only in the degenerate combination  $\beta = \Omega_0^{0.6}/b$  where  $b$  is the linear bias parameter (e.g. Kaiser 1987; Hamilton 1992; Fisher, Scharf & Lahav 1994; Heavens & Taylor 1995;

Ballinger, Heavens & Taylor 1995; Cole, Fisher & Weinberg 1995). The current values for  $\beta$  fall roughly in the range 0.5-1 depending on the measurement method used and on the catalogue selection criteria (Strauss & Willick 1995; Hamilton 1997). Even if  $\beta = 0.5$ ,  $\Omega_0$  could still be close to its critical value if dark matter is poorly traced by luminous objects. The determination of the density parameter from linear peculiar velocities or redshift space distortion studies is therefore compromised by the lack of a good measurement of the bias parameter. This motivates methods which attempt to measure  $\Omega_0$  directly (Dekel & Rees 1994; Fan, Bahcall & Cen 1997) or methods to determine  $b$ , which then allows determination of  $\Omega_0$  from  $\beta$ . In this paper, we pursue the latter approach: there is a relative bias between IRAS and optically selected galaxies (e.g. Peacock 1997), so at least one of the galaxy types must be at best a biased tracer of the underlying mass distribution. In practice, we have very little idea of how bias works and evolves, and there is therefore strong motivation to measure it empirically from the galaxy distribution. Future Cosmic Microwave Background experiments may allow the simultaneous determination of

all the main cosmological parameters with unprecedented accuracies (Jungman et al. 1996; Bersanelli et al. 1996), in which case the major motivation of studies like this will be to constrain galaxy formation mechanisms and the power spectrum by measuring  $b$  directly, rather than, as here, on using it as a route to  $\Omega_0$ .

In a previous paper (Matarrese et al. 1997; hereafter MVH97) we presented a method to measure the bias parameter from LSS data by studying higher-order characteristics of the density field. We developed an idea of Fry (1994): since the degeneracy between  $b$  and  $\Omega_0$  is an intrinsic feature of linear theory, one needs to go to second order to separate the parameters. Under the assumption that the initial fluctuation field is Gaussian and that structures grow by gravitational instability, the three-point correlation function and its counterpart in Fourier space, the bispectrum, are intrinsically second order quantities. The bispectrum has the advantage that the range of validity of perturbation theory appears well-defined (Scoccimarro et al. 1998) - if the power spectrum is roughly known - and in the appropriate range, the correlation properties of the estimators can be calculated. If the bias is local, this allows us to estimate it via a likelihood method, and therefore to assign an errorbar. For consistency with second order perturbation theory (2OPT) the first non-linear bias term must also be considered, and this can introduce an additional degeneracy between skewness induced by gravitational evolution and that introduced by bias. The two effects can, however, be separated by the use of shape information: essentially non-linear biasing of a truly Gaussian field will lead to different shaped structures from a non-Gaussian field arising from gravitational instability. Since the signal comes from the mildly non-linear regime, the bias can be measured on scales where  $\Delta^2$  (the conventional variance per unit logarithmic interval) is about unity. In MVH97 we showed that the bispectrum method we presented succeeds in recovering the true value for the bias with a reasonable error in a very idealized case where the positions of the particles were known in real space. In reality, the best distance indicator for large galaxy catalogues is redshift; the main purpose of this paper is to show how the bispectrum in redshift-space can be used to estimate bias.

Galaxy catalogues use the redshift as third spatial coordinate. In a perfectly homogeneous Friedman Universe, redshift would be an accurate distance indicator, but inhomogeneities perturb the Hubble flow, and introduce peculiar velocities. The resulting redshift-space map of the galaxy distribution is thus distorted. As Kaiser (1987) pointed out, peculiar velocities distort the clustering pattern in redshift space on all scales, but the effect can be regarded as being split into two components: a large-scale distortion resulting from coherent inflow into over-dense regions, and the ‘Fingers-of-God’ (FoG) arising from virialised, highly non-linear structures. For the bispectrum, we find distortions in redshift-space arising in 2OPT (cf. Hivon et al. 1994), but also significant effects from virialised structures. In this paper, we incorporate the effects of virialised structures by a method which has been successfully used with the redshift-space power spectrum: we model the effects as an incoherent velocity dispersion. Once again the shape information allows the disentanglement of redshift space distortions and other effects: redshift-space mapping modifies the shape of

the structures in a different way from gravitational evolution and biasing.

The next generation of galaxy surveys, like for example the Anglo-Australian 2-degree Field (2dF, Colless 1996) and Sloan Digital Sky Survey (SDSS, Gunn & Weinberg 1995), will allow not only accurate measurement of  $\beta$ , but also estimation of the bias parameter with an accuracy of a few percent.

This paper is principally concerned with the treatment of redshift distortions; a subsequent paper will present a detailed study of the other issues.

The plan of this paper is as follows. In Section 2 we quantify the effect that redshift distortions have on the bispectrum, and, as a consequence, on the determination of the bias parameter. Then we present a second-order perturbation description for the effect of redshift distortions on the bispectrum and on the covariance matrix needed for the likelihood analysis. Also we discuss how to include the modelling of small scale, highly non-linear effects, such as FoG: non-linear dynamics and virialised structures in redshift space contaminates scales that in real space would be only mildly non-linear. Section 3 contains the practical implementation of the method in a numerical simulation of the redshift space galaxy distribution. In Section 4 we discuss the applicability of the method in more general terms: we implement the analysis on an open Universe simulation and on a biased distribution in real space. The results obtained from the unbiased and the biased distributions are also shown. Section 5 discusses the results also in the prospect of the next generation of large galaxy redshift surveys.

## 2 MODELLING OF REDSHIFT DISTORTIONS

It is worth making a few remarks about performing this sort of analysis in Fourier space. Fourier space analysis has the great advantage that there is a clear separation of scales where perturbation theory works and breaks down. Given the nature of the redshift distortion however, the natural way would be to decompose the density field in spherical harmonics and spherical Bessel functions (Heavens & Taylor 1995). But, we showed in MVH97, rather than using the survey as a whole, it is more effective to split it into subsamples. For a deep survey in the individual subsamples the Fourier decomposition and Kaiser’s (1987) distant observer approximation to model even large-scale distortions is a good description.

### 2.1 Effects of redshift distortions on the power spectrum and on the bispectrum

As a preliminary, in this section we compute the effects of redshift distortion on a particularly simple class of bispectra, those whose wavevectors form an equilateral triangle and averaging over orientation. This analysis is not required in later sections, but serves to illustrate the effects of perturbation theory and the virialisation model.

On large (linear) scales the redshift space effect on an individual Fourier component of the density fluctuation field  $\delta_{\vec{k}}$  can be described as:

$$\delta_{\vec{k}} \longrightarrow \delta_{\vec{k}}^s = \delta_{\vec{k}}(1 + \beta\mu^2), \quad (1)$$

where the superscript  $s$  refers to the quantity in redshift space, and  $\mu$  is the cosine of the angle between the  $k$ -vector and the line of sight (i.e. the direction along which the distortion takes place). Throughout, we adopt the distant-observer approximation, so  $\mu$  is independent of location within the survey.

The effect on the average power spectrum in a thin shell in  $k$ -space is:

$$\langle \delta_{\vec{k}} \delta_{\vec{k}^*} \rangle \longrightarrow \left(1 + \frac{2}{3}\beta + \frac{1}{5}\beta^2\right) \langle \delta_{\vec{k}} \delta_{\vec{k}^*} \rangle. \quad (2)$$

This is an enhancement of the redshift space power on all scales by the same factor,  $28/15$  in the case where  $\beta = 1$ .

The bispectrum  $B(\vec{k}_1, \vec{k}_2, \vec{k}_3) \propto \langle \delta_{g\vec{k}_1} \delta_{g\vec{k}_2} \delta_{g\vec{k}_3} \rangle$  is non-zero only if the 3 wavevectors form a closed triangle. For equilateral triangles, averaging the three factors in equation (1) over  $\mu$  gives

$$B^s = \left(1 + \beta + \frac{3}{5}\beta^2 + \frac{1}{7}\beta^3\right) B, \quad (3)$$

so that for  $\beta=1$  there is an amplification of the bispectrum on all scales by a factor  $B^s/B = 96/35$ .

We can estimate the effect of redshift distortions on the estimation of the bias parameter by noting that, in the absence of shot noise and a non-linear bias term,  $b \propto P^2/B$  (MVH97). If redshift distortions are ignored, the bias parameter is overestimated by a factor

$$\frac{(P^s/P)^2}{B^s/B} = 1.27, \quad (4)$$

if  $\beta = 1$ .

Virialised motion produces a radial smearing and the associated FoG effect contaminates the wavelengths we are interested in. This is hard to treat exactly, but being a smearing effect it produces a mild damping on the power acting in the opposite direction to the large-scale boosting of power (see for example Matsubara 1994). A model was introduced by Peacock (1992; see also Peacock & Dodds 1994) in which the small scale velocity field is assumed to have an incoherent Gaussian distribution. In reality, according to evidence from simulations (e.g. Zurek et al. 1994) and observations (e.g. Marzke et al. 1995) the velocity distribution is better modelled by an exponential, but in practice there is very little difference between these two models on scale where the damping factor is  $\leq 2$  (Ballinger, Peacock & Heavens 1996). In practice this incoherent model fits well the power spectrum in numerical simulations (Hatton & Cole 1998).

In the Fourier domain the exponential velocity dispersion model gives a damping factor  $D(k\sigma\mu)$  (where  $k \equiv |\vec{k}|$ ), such that  $\delta_{\vec{k}} \longrightarrow \delta_{\vec{k}} D$ , given by

$$D(k\sigma\mu) = \frac{1}{\sqrt{1 + k^2\sigma^2\mu^2/2}}, \quad (5)$$

where  $\sigma$  is the pairwise velocity dispersion of galaxies. The overall effect in  $k$ -space can be obtained by multiplying the large-scale enhancing factor and the small-scale damping factor before averaging over  $\mu$  (Peacock & Dodds 1994):

$$\delta_{\vec{k}} \longrightarrow \delta_{\vec{k}} \frac{(1 + \beta\mu^2)}{\sqrt{1 + k^2\sigma^2\mu^2/2}}. \quad (6)$$

For the power spectrum in a thin shell in  $k$ -space the overall

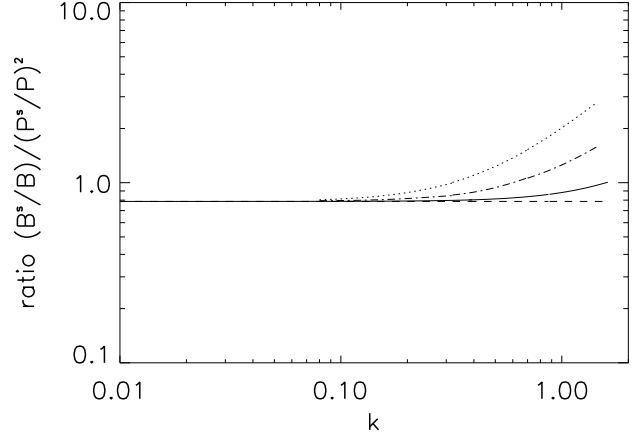


**Figure 1.** Scale dependence of the redshift distortions on the measurement of the bias parameter, which is overestimated by 1/ordinate if the distortions are ignored. The dashed line refers to the case where there is no small scale velocity dispersion ( $\sigma = 0$ ), the solid line is for  $\sigma = 200 \text{ km s}^{-1}$ , the dot-dashed line is for  $\sigma = 400 \text{ km s}^{-1}$  and the dotted line is for  $\sigma = 700 \text{ km s}^{-1}$ . The wavenumber  $k$  is in units of  $h \text{ Mpc}^{-1}$ .

effect is given by:

$$P^s(k) = \left\{ 4 \frac{(\sigma^2 k^2 - \beta)\beta}{\sigma^4 k^4} + \frac{2\beta^2}{3\sigma^2 k^2} + \frac{\sqrt{2}(k^2\sigma^2 - 2\beta)^2 \arctan(k\sigma/\sqrt{2})}{k^5\sigma^5} \right\} P(k). \quad (7)$$

Similarly for the angle-averaged bispectrum for equilateral triangles one obtains

$$B^s(k) = \left\{ \frac{2k^6\sigma^6 - 12k^4\sigma^4\beta + (36k^2\sigma^2 + 6k^4\sigma^4)\beta^2}{\sqrt{2}k^6\sigma^6\sqrt{2} + k^2\sigma^2} + \frac{(k^4\sigma^4 - 5k^2\sigma^2 - 30)\beta^3}{\sqrt{2}k^6\sigma^6\sqrt{2} + k^2\sigma^2} + \frac{3\sqrt{2}\beta(2k^4\sigma^4 - 6k^2\sigma^2\beta + 5\beta^2) \operatorname{arcsinh}(k\sigma/\sqrt{2})}{k^7\sigma^7} \right\} B(k). \quad (8)$$

The overall effect on the measurement of the bias parameter is given by the ratio [equation (4)]. In the case  $\beta = 1$  (that, since  $\beta$  is expected to be  $\leq 1$ , is the case where large-scale redshift distortions are most important) the scale dependence of this quantity is shown in Fig. 1. For small velocity dispersions the effect is small for a reasonable range of  $k$ -vectors, but for bigger  $\sigma$  it diverges quite quickly. Since we expect to use wavelengths up to  $k \simeq 2$  (throughout the  $k$  unit is  $h \text{ Mpc}^{-1}$ ) in order to have a good signal to noise, ignoring redshift distortions introduces unacceptably big errors. In the next section we illustrate a more elegant way to deal with this problem and to have a more satisfactory

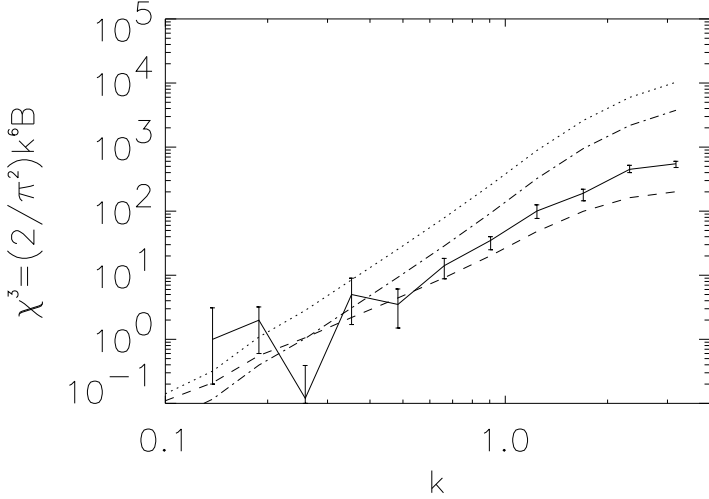


**Figure 2.** Redshift distortions effects on the bispectrum. The bispectrum is expressed in the dimensionless form  $\chi^3$  that is the counterpart for the bispectrum of  $\Delta^2$  for the power spectrum:  $\chi^3 \equiv (2/\pi^2)^2 k^6 B$ , where  $k$  is the smallest wavenumber in the triangle. The dot-dashed line is the 2OPT-real space bispectrum, the dotted line is the redshift-space bispectrum obtained taking into account only the large scale boosting effect, the dashed line is the 2OPT bispectrum with the small scale smoothing effect included as in equation (8). The velocity dispersion used here ( $\sigma = 650 \text{ km s}^{-1}$ ) is the one that gives the best fit to the redshift-space power spectrum up to  $k \simeq 0.8$ . Finally the thick solid line with errorbars is the measured bispectrum from the redshift-space map. The agreement up to  $k \simeq 0.7$  should be compared with the corresponding breakdown of 2OPT in real-space ( $k = 0.55$ ; MVH97). As before  $k$  is in units of  $h \text{ Mpc}^{-1}$ .

result: the redshift distortions should be modelled for consistency to second order using perturbation theory and the small scale effect cannot be neglected.

The redshift-space effect on the bispectrum from equilateral triangles is illustrated in Fig. 2, which shows results from an N-body simulation by the Hydra consortium (Couchman et al. 1995). It is a cold dark matter (CDM) simulation with  $\Omega_0 = 1$ , a shape parameter  $\Gamma = 0.25$ ,  $\sigma_8 = 0.64$ , no cosmological constant and no biasing.

## 2.2 Second-order perturbation description for the effect of redshift distortions

In the framework of second order perturbation theory (2OPT) for the density field, for consistency also redshift distortions should be treated to second order. Unfortunately highly non-linear effects contaminate scales where 2OPT should hold. This can be easily understood by considering how a spherical over-density appears distorted by peculiar velocities when observed in redshift space (in the small angle approximation). At large scales (linear regime) the collapsing shells appear squashed, the squashing increases until the infall velocity cancels with the Hubble expansion. At this point, where the dynamics is only mildly non-linear, the region appears to be collapsed on a sheet of infinite density in redshift space. At smaller scales the collapsing regions

and the already virialised (highly non-linear) regions appear elongated along the line of sight (FoG). From equation (6) it is clear that the damping factor acts as a filter on the Fourier components of the density field. Therefore our analysis involves 2OPT of the density field and of the redshift distortions combined with the exponential model for small scale velocity dispersions acting as a smoothing filter.

## 2.3 Large-scale second order model

We assume a local correspondence between the galaxy overdensity field  $\delta_g$  and the underlying mass density field  $\delta \equiv \delta\rho/\rho$ , and make a Taylor expansion in  $\delta$ :

$$\delta_g = \sum_i \frac{b_i}{i!} \delta^i, \quad (9)$$

retaining terms to  $i = 2$ , but ignoring  $i = 0$  as it contributes only to  $k = 0$ .

The bispectrum  $B$  is defined by the 3-point function in Fourier space:

$$\langle \delta_{g\vec{k}_1} \delta_{g\vec{k}_2} \delta_{g\vec{k}_3} \rangle = (2\pi)^3 B(\vec{k}_1, \vec{k}_2, \vec{k}_3) \delta^D(\vec{k}_1 + \vec{k}_2 + \vec{k}_3), \quad (10)$$

where  $\delta^D$  is a 3D Dirac delta function. The expression for  $B$  is given in MVH97 for  $\delta$  in real space. In redshift space, the bispectrum is inevitably more complicated (Heavens et al., in preparation):

$$\begin{aligned} B(\vec{k}_1, \vec{k}_2, \vec{k}_3) = & b_1^2 (1 + \mu_1^2 \beta) (1 + \mu_2^2 \beta) \\ & \left\{ [2P(\vec{k}_1)P(\vec{k}_2)\text{Ker}(\vec{k}_1, \vec{k}_2, \beta, \mu_1, \mu_2, \mu) + \text{cyc.}] \right. \\ & \left. + b_2 [P(\vec{k}_1)P(\vec{k}_2) + \text{cyc.}] \right\}, \end{aligned} \quad (11)$$

where the cyclic terms are (1,3) and (2,3), and

$$\begin{aligned} \vec{k}_3 &= -\vec{k}_1 - \vec{k}_2, \\ \mu_i &= \frac{\vec{r} \cdot \vec{k}_i}{r k_i}, \\ \mu &= -\mu_3. \end{aligned} \quad (12)$$

The kernel is given by

$$\begin{aligned} \text{Ker}(\vec{k}_1, \vec{k}_2, \beta, \mu_1, \mu_2, \mu) \equiv & J(\vec{k}_1, \vec{k}_2) b_1 + \mu^2 \beta b_1 K^{(2)}(\vec{k}_1, \vec{k}_2) + \mu_1^2 \mu_2^2 \beta^2 b_1^2 + \\ & \frac{b_1^2 \beta}{2} (\mu_1^2 + \mu_2^2) + \frac{b_1^2 \beta}{2} \mu_1 \mu_2 \left( \frac{k_1}{k_2} + \frac{k_2}{k_1} \right) + \\ & \frac{b_1^2 \beta^2}{2} \mu_1 \mu_2 \left( \mu_2^2 \frac{k_2}{k_1} + \mu_1^2 \frac{k_1}{k_2} \right), \end{aligned} \quad (13)$$

where the real-space kernel is (e.g. Catelan & Moscardini 1994a)

$$\begin{aligned} J(\vec{k}_1, \vec{k}_2) \equiv & \frac{5}{7} + \frac{\vec{k}_1 \cdot \vec{k}_2}{2k_1 k_2} \left( \frac{k_1}{k_2} + \frac{k_2}{k_1} \right) + \frac{2}{7} \left( \frac{\vec{k}_1 \cdot \vec{k}_2}{k_1 k_2} \right)^2 \end{aligned} \quad (14)$$

and  $K^{(2)}$  comes from the velocity field (e.g. Catelan & Moscardini 1994b)

$$\begin{aligned} K^{(2)}(\vec{k}_1, \vec{k}_2) = & \frac{3}{7} + \frac{\vec{k}_1 \cdot \vec{k}_2}{2k_1 k_2} \left( \frac{k_1}{k_2} + \frac{k_2}{k_1} \right) + \frac{4}{7} \left( \frac{\vec{k}_1 \cdot \vec{k}_2}{k_1 k_2} \right)^2. \end{aligned} \quad (15)$$

In real space the 2OPT bispectrum is very weakly dependent on  $\Omega_0$  (e.g. MVH97). In redshift space, there is a strong  $\Omega_0$ -dependence, but only via  $\beta$ , which can be measured from the power spectrum. The residual dependence on  $\Omega_0$  is again very weak, and we therefore quote the results for  $\Omega_0 = 1$ .

We wish to write  $B$  in terms of observable quantities, which  $P$  is not. To the order which we are working, we may write  $P = P_g/b_1^2$ . There are one-loop corrections to this which may be significant if  $b_2$  and  $b_3$  are not close to zero (Heavens et al. in preparation). In Section 4 we investigate the practical effects of those corrections using biased simulations, but consistently with perturbation theory, in terms of the real-space galaxy power spectrum  $P_g = b_1^2 P$ , we can write:

$$\langle \delta_{g\vec{k}_1} \delta_{g\vec{k}_2} \delta_{g\vec{k}_3} \rangle^s = \mathcal{G}(P_g, \beta, c_1, c_2, \vec{k}_1, \vec{k}_2, \vec{k}_3), \quad (16)$$

where

$$\begin{aligned} \mathcal{G}(P_g, \beta, c_1, c_2, \vec{k}_1, \vec{k}_2, \vec{k}_3) = & \\ & (2\pi)^3 (1 + \beta\mu_1^2)(1 + \beta\mu_2^2) \\ & \{ c_1 [2P_g(\vec{k}_1)P_g(\vec{k}_2)\text{Ker}(\vec{k}_1, \vec{k}_2, \beta, \mu_1, \mu_2, \mu) + \text{cyc.}] \\ & + c_2 [P_g(\vec{k}_1)P_g(\vec{k}_2) + \text{cyc.}] \} \delta^D(\vec{k}_1 + \vec{k}_2 + \vec{k}_3), \end{aligned} \quad (17)$$

where the parameters we wish to extract  $b_1$ ,  $b_2$  appear in the combinations

$$c_1 \equiv \frac{1}{b_1}; \quad c_2 \equiv \frac{b_2}{b_1^2}. \quad (18)$$

It is interesting to notice here that the degeneracy between  $\Omega_0$  and  $b$  can be lifted because equation (13), as explained before, is dependent on  $\Omega_0$  mostly through the measurable parameter  $\beta$  and is quite insensitive to  $\Lambda$  (see also Bernardeau 1994; Eisenstein 1997); the error introduced by neglecting the  $\Omega$ - and  $\Lambda$ -dependence of the bispectrum is much smaller than the final expected error in the determination of the bias parameter, and can therefore be safely ignored for this purpose. Redshift-space distortions may also be introduced by a separate effect, arising from an incorrect geometry being used to create the redshift-space map (Phillips 1994; Ballinger et al. 1996). This effect should be detectable with SDSS and corrected for. This accounts for the large-scale effects via perturbation theory. We now turn to the effects of small-scale velocities.

## 2.4 Small scale model

It is worth noticing that the model of small-scale velocity dispersion is simplistic because it takes no account of the fact that the velocity dispersion is correlated with the density field. This means that the dispersion is higher in high density regions such as galaxy clusters. The value  $\sigma$  used in the model (equation 6) is therefore only an ‘‘effective’’ velocity dispersion which depends on how galaxies populate the clusters and on the bias parameter  $b$  (Fisher 1995). In principle, the form of the filtering may be unconnected with the small-scale velocity distribution, because the modelling assumes that the velocity is uncorrelated with the density, which is untrue in detail. In practice, then, one should perhaps treat the filter function as a heuristic object whose

parameter  $\sigma$  is determined from the large-scale data, by fitting the power spectrum. A Taylor expansion as  $k \rightarrow 0$  will demand a quadratic form for  $D \simeq 1 - k^2\sigma^2\mu^2/4 + O(k^4)$ , so one might expect the model to be generally good provided  $k^2\sigma^2\mu^2$  is small. We have found this to be the case for the power spectrum; in high- $\Omega_0$  models, imposing a limit of  $\alpha = k^2\mu^2 = 0.3$  works well (for a CDM model with  $\Omega_0 = 1$ ,  $\sigma_8 = 0.64$  and  $\Gamma = 0.25$ ).

The small scale damping effect acts as a smoothing filter (see equation 6) on the non-linear field. Following the general mathematical method outlined in Section 3 of MVH97 for calculating  $N$ -point distributions in Fourier space it is possible to obtain an expression for the galaxy  $N$ -point spectra in redshift space that includes the large scale effect to second order in perturbation theory (equation 11) and the small-scale effect due to the velocity dispersion of the galaxies (equation 5). The technical derivation can be found in Appendix A. For  $N = 3$ , as a special case we obtain the final expression for the galaxy bispectrum in redshift space for a given triangle configuration, that also includes small scale velocity dispersion:

$$\begin{aligned} \langle \delta_{g\vec{k}_1} \delta_{g\vec{k}_2} \delta_{g\vec{k}_3} \rangle^s = & \\ & \frac{\mathcal{G}(P_g, \beta, c_1, c_2, \vec{k}_1, \vec{k}_2, \vec{k}_3)}{\sqrt{(1 + \vec{k}_1^2\sigma^2\mu_1^2/2)(1 + \vec{k}_2^2\sigma^2\mu_2^2/2)(1 + \vec{k}_3^2\sigma^2\mu_3^2/2)}}, \end{aligned} \quad (19)$$

where  $\mathcal{G}$  is given by equation (17).

This is also the key equation of this paper, generalising MVH97 to redshift space galaxy catalogues. Note that we assume that  $\beta$  and  $\sigma$  (and hence  $P_g(k)$  in real space) are computed directly from the redshift-space power spectrum  $[P_g^s(\vec{k})]$ , so they are not parameters to be determined from the bispectrum (see section 3.1).

In order to be able to perform the likelihood analysis the covariance matrix for the bispectrum has to be consistently modified. The covariance matrix for the bispectrum involves the expression for the six-point function as shown in equations (15) and (16) of MVH97.

Referring to equations (38) to (42) of MVH97, we will quote here how to modify the equations when working in redshift space:

$$P(\vec{k}) \longrightarrow P(\vec{k})(1 + \beta\mu^2)^2 \quad (20)$$

(in the power spectrum only, not the bispectrum below);

$$\langle \delta_{g\vec{k}_1} \delta_{g\vec{k}_2} \delta_{g\vec{k}_3} \rangle \longrightarrow \mathcal{G}(P_g, \beta, c_1, c_2, \vec{k}_1, \vec{k}_2, \vec{k}_3). \quad (21)$$

And finally the covariance matrix  $C_{\alpha\beta}$  obtained with this prescription needs to be filtered:

$$C_{\nu_1\nu_2} \longrightarrow \frac{C_{\nu_1\nu_2}}{\sqrt{\prod_{i=1}^6 (1 + k_i^2\sigma^2\mu_i^2/2)}}, \quad (22)$$

where the index  $i$  runs over the six vectors that form the two triangles  $\nu_1$  and  $\nu_2$ .

## 3 TESTS ON N-BODY SIMULATIONS

We have tested the model (equations 19 & 22) by performing a likelihood analysis of the bispectrum on an unbiased redshift-space catalogue created from an  $N$ -body simulation

provided by the Hydra consortium (Couchman et al. 1995). This is a CDM simulation with  $\Omega_0 = 1$ ,  $\sigma_8 = 0.64$  and  $\Gamma = 0.25$ ; these parameters have been chosen to match closely the present day galaxy power spectrum. It is clear from equations (11), (17) and (19) that in a realistic application we need to know (or have an accurate fit for) the real space galaxy power spectrum, because it is this quantity that is required in the model and, knowing it, subsequently we can attempt to evaluate  $\sigma$ .

Therefore, as a first step, we need to know if we are able to reconstruct the real-space galaxy power spectrum. The problem is greatly complicated by the fact that the method is applied on individual subvolumes, rather than on the overall volume. Even assuming that the data will be good enough to enable us to reconstruct the real-space power spectrum for the whole volume of the survey, some care is needed in extracting then the real space spectrum for each subsample. A subsequent paper will focus on this issue, in the present paper we shall assume that we have an accurate enough fit for the real space power spectrum. In Appendix B we give some limits on the accuracy needed.

### 3.1 Limit of validity of the small scale redshift distortion model

As mentioned in Section 2.4, the value  $\sigma$  used in the model is only an “effective” velocity dispersion, so it can actually be seen as a parameter whose value is fixed by the condition that equation (6), when applied to the real space Fourier modes, gives the observed redshift space power spectrum. The limit of validity of the model, i.e. the maximum value of  $\alpha = k^2\mu^2$ , can be set as follows.

Since we can assume, as seen in Section 2.4, that the real-space power spectrum is known, a likelihood analysis of the redshift space Fourier modes should give the two parameters  $\beta$  and  $\sigma$ .

The probability distributions of the real and imaginary parts of  $\delta_{\vec{k}}$  are Gaussian in linear theory, but the second order correction induces skewness. However in this regime the contribution from the second order correction is relatively small, and in any case, the Central Limit Theorem ensures that the average of a set of modes from a region in  $k$ -space will tend to a gaussian for a large number of modes, and the likelihood for the set is then equivalent to a product of individual gaussians, since homogeneity alone ensures that the modes are uncorrelated. Therefore, the likelihood tends to a product of Gaussians with zero means and dispersion  $\sqrt{P^s(k, \mu)}/2$ , where

$$P^s(k, \mu) = P(k)(1 + \beta\mu^2)^2 D(k\sigma\mu)^2. \quad (23)$$

The combined likelihood for  $\beta$  and  $\sigma$

$$\mathcal{L}(\beta, \sigma) = \frac{1}{(2\pi)^{M/2} \prod_{\nu} (\frac{1}{2} P^s(k, \mu))} e^{-\frac{1}{2} \sum_{\nu} \frac{\{\text{Re } \delta_{\vec{k}}\}^2 + \{\text{Im } \delta_{\vec{k}}\}^2}{\frac{1}{2} P^s(k, \mu)}}. \quad (24)$$

The parameter  $\beta$  in the simulation is known, but also in a realistic application will be known through an independent method (see the Introduction), therefore we can say that the modelling for the small scale velocity dispersion effect

breaks down where the likelihood fails to recover the “true” value for  $\beta$ . On large scales the model is expected to be valid for any value of the factor  $\alpha = k^2\mu^2$ , but on smaller scales  $\alpha$  must be constrained. We find no constraint on  $\alpha$  up to  $k = 0.70$  then  $\alpha < 0.3$  up to  $k = 0.9$ . For higher  $k$  it becomes difficult to have a constraint on both  $\beta$  and  $\sigma$  for any value of  $\alpha$ . This feature is a direct consequence of an effect noted also by Bromley, Warren & Zurek (1997): at short wavelengths the  $\mu$  dependence is cancelling. However for  $k > 0.9$   $\sigma$  can still be recovered with less than 5 per cent uncertainty keeping  $\alpha \leq 0.3$  and constraining  $\beta$  to assume the value previously determined.

We notice a slight increase of the value for  $\sigma$  with  $k$ . This would suggest that the exponential model is not exact, but, as we already pointed out,  $\sigma$  can be treated as an empirical parameter.

### 3.2 Obtaining the effective velocity dispersion in the subvolumes

In the individual subvolumes the power spectrum becomes noisier, and the large-scale modes are not well sampled. Assuming that the local real space power spectrum is known, we can determine the local  $\sigma$ , because the local value for  $\beta$  can be extrapolated from the global one as follows: if  $N_{SV}^s$  is the number of particles in the subvolume in redshift space and  $N_{\text{tot}}$  is the number of particles in the whole volume of the sample

$$\beta_{\text{local}} = \beta_{\text{global}} \left( \frac{N_{SV}^s}{N_{\text{tot}}} \right)^{0.6}. \quad (25)$$

There is a subtlety to point out here: in principle we would need to use the number of particles in the real space subvolume, but this is not known. However if the subsamples are not too small it should not make too much difference due also to the degeneracy that arises on those scales between  $\beta$  and  $\sigma$ . Moreover an error of 20 per cent in the mean density (that is the biggest fluctuation we observe in splitting our simulation of  $100h^{-1}$  Mpc side in subsamples of  $50h^{-1}$  Mpc side) leads to an error of 5 per cent on  $\beta_{\text{local}}$  that is of the same order of the uncertainty on  $\sigma$  obtained from the likelihood.

Since we noticed a slight increase on the value for  $\sigma$  with  $k$ , the value for  $\sigma$  has been obtained independently for different intervals of  $k$ .

We performed a likelihood analysis as described above, with  $\beta$  fixed, to recover  $\sigma$  for each subvolume, in bands of  $k$  limited by the following values: 0.3, 0.7, 0.85, 1.0, 1.2, 1.3, with an additional band 1.7 – 2.6.

The reason for this choice of intervals will be evident in the next section.

## 4 LIKELIHOOD ANALYSIS

It is evident from (19) that a set of triangles in  $k$ -space allows the measurement of the bias parameters  $b_1$  and  $b_2$  through a likelihood analysis. It is however necessary to consider triangles of different shapes in order to lift a new degeneracy between  $b_1$  and  $b_2$  since a set of triangles of the same shape gives almost degenerate information on  $b_1$  and  $b_2$  while for

the equilateral triangles the degeneracy is complete. The optimal triangle configurations are not easy to determine, but it is particularly effective to consider, along with equilateral triangles, a configuration consisting of a repeated vector and one of twice the amplitude and opposite direction (referred to as ‘degenerate’). By ensuring that any  $\vec{k}$  appears in only one triangle of either shape (and  $-\vec{k}$  does not appear elsewhere either) the data are uncorrelated (MVH97): the covariance matrix is diagonal and the likelihoods for different shapes can be multiplied. This simplifies the likelihood analysis considerably.

## 4.1 Choice of $k$ -vector limits

### 4.1.1 $\Omega_0 = 1$ Universe

Due to the smearing effect of small scale velocities the range of validity of 2OPT is expected to be slightly extended. This is exactly what we observe. For equilateral configurations for example, from Fig. 2 it is clear that the redshift-space bispectrum for equilateral triangles is well described by our model up to  $k \simeq 0.7 - 0.9$ .

In real space the  $k$ -vector range we used for the likelihood analysis of the bispectrum was:  $0.3 \leq k < 0.55$  for equilateral configurations, and  $0.55 \leq k_{\text{short}} < 1.1$  for degenerate. In the redshift-space likelihood analysis for the bispectrum the range of  $k$ -vector used changes: for equilateral configurations  $0.3 \leq k < 0.85$  and, for degenerate configuration,  $0.85 \leq k_{\text{short}} < 1.3$ .

### 4.1.2 Low- $\Omega_0$ Universe

In real-space the second-order bispectrum is only weakly dependent on  $\Omega_0$  (e.g. MVH97), in redshift-space there is an additional dependence on  $\Omega_0$ , but this is only through the parameter  $\beta$  that can be measured (Heavens et al. in preparation). Although the remaining dependence on  $\Omega_0$  is very weak, in a real survey we need to decide *a priori* where to place the upper cutoff in wavenumber. Since, in principle, this will be dependent on  $\Omega_0$ , we investigate a low-density numerical simulation to see how robust the cutoff wavenumber is. The simulation, again from the Hydra Consortium, is for a CDM model with parameters  $\Omega_0=0.3$ ,  $\Lambda = 0$ ,  $\Gamma=0.25$ , and a box-size of  $100 h^{-1}$  Mpc. Fig. 3 shows how the real space likelihood contour for  $c_1$  and  $c_2$  varies with the cutoff wavenumber for this simulation. This final output has  $\sigma_8=1.06$ , which makes it unsuitable for our redshift-space analysis. In fact the real space analysis recovers the true value for the bias within the errors ( $c_1 = 0.9 \pm 0.5$ ,  $c_2 = 0.1 \pm 0.7$ ) but the first mildly non-linear wavelengths are larger than the box and the redshift-space distortions are too non-linear for the wavelengths we need to use. We have therefore analysed two earlier epochs, with  $\sigma_8 = 0.64$  (when  $\Omega_0 = 0.5$ ) and  $\sigma_8 = 0.81$  (when  $\Omega_0 = 0.41$ ).

For the redshift-space analysis in these cases, since there is a strong covariance between  $\beta$  and  $\sigma$ , it was not always possible for all the  $k$ -vector bands to follow the procedure outlined in Section 3 to set the values for the velocity dispersion parameter  $\sigma$  and the angle  $\alpha$ . When it was not possible to close the likelihood contours for  $\beta$  and  $\sigma$ , we assumed  $\beta$  was known to set the value for  $\sigma$  and we used for  $\alpha$  the same constraint as in the other cases. We also find that the

method for the redshift space analysis recovers the true value of the bias parameter within the errors. The errors are still big (100 per cent), but the non-linear scale is also quite big ( $k < 0.3$ ) and we can reduce the errors by analyzing subvolumes (MVH97). A rough estimate for the number of volumes that one can obtain from the SDSS (about a thousand if linear theory breaks down at  $k_{\text{nl}} \simeq 0.1$ , about eight thousand if  $k_{\text{nl}} \simeq 0.3$ ) suggests that an accuracy of few percent or better should be achieved.

### 4.1.3 General case

The range of validity of second order perturbation theory depends on the model of the Universe, so we therefore need to be able to determine, in a consistent manner, where 2OPT breaks down prior to estimating  $\Omega_0$ . For all the simulations we analyzed the breakdown occurs where the real-space normalized bispectrum  $\chi^3 = (2/\pi^2)k^6 B$  (analogous to the quantity  $\Delta^2$  for the power spectrum) is  $\chi^3 \simeq 10$  for equilateral triangles, and  $\simeq 100$  for degenerate triangles. This real-space quantity can be estimated, assuming, as we do, that  $\beta$  and the small-scale velocity dispersion  $\sigma$  can be estimated from the redshift-space power spectrum. For the two earlier epochs of the low- $\Omega_0$  simulation we also changed  $\sigma_8$  by reinterpreting the box size (e.g. Mann, Peacock & Heavens 1997): also in these cases the breakdown occurs for the same values of the normalized bispectrum  $\chi^3$ .

## 4.2 Biased catalogue

In order to create a biased catalogue, we applied the standard friends-of-friends algorithm to the same  $\Omega_0 = 1$  N-body simulation used in MVH97 and in Section 2.1. We adopted a linking parameter equal to 15 per cent of the mean interparticle distance, i.e. approximately  $0.12h^{-1}$  Mpc. The biased catalogue is defined as the list of all the groups of particles with at least three members; the corresponding number density is  $5.6 \times 10^{-2} h^3 \text{ Mpc}^{-3}$ . Although this density is more realistic than that of the unbiased catalogue ( $2.1 h^3 \text{ Mpc}^{-3}$ ) used in MVH97 and in the redshift-space analysis, this is still about six times larger than the number density that future galaxy surveys will have, but with this choice shot noise does not dominate the signal in the regime where 2OPT should hold, allowing a determination of the breakdown of 2OPT.

This biasing scheme is not necessarily equivalent to the high peaks biasing scheme nor can necessarily be analytically expressed as in equation (9). However for the purpose of recovering  $\Omega_0$  from the  $\beta$  parameter what is necessary is the ‘effective bias’  $b_{\text{eff}}$  defined as:  $P_g = b_{\text{eff}}^2 P$ . In the biased catalogue  $b_{\text{eff}} = 1.1$  on scale where 2OPT holds.

Also in presence of biasing the breakdown of 2OPT can easily be detected. Fig. 4 shows how the joint likelihood contours vary for  $k$ -vectors of the degenerate triangle configuration belonging to different independent shells in  $k$ -space. It is clear that 2OPT breaks down at  $k \simeq 0.8$ . When perturbation theory breaks down the likelihood does not drift in a precise direction as it happens for the unbiased case. This can be due to the superposition of the non-linear clustering (that drifts the likelihood towards high  $c_1$ ) and the biasing acting in the opposite direction. For the biased case the  $k$ -vector limits are for the equilateral configuration  $0.3 < k < 0.5$  and for

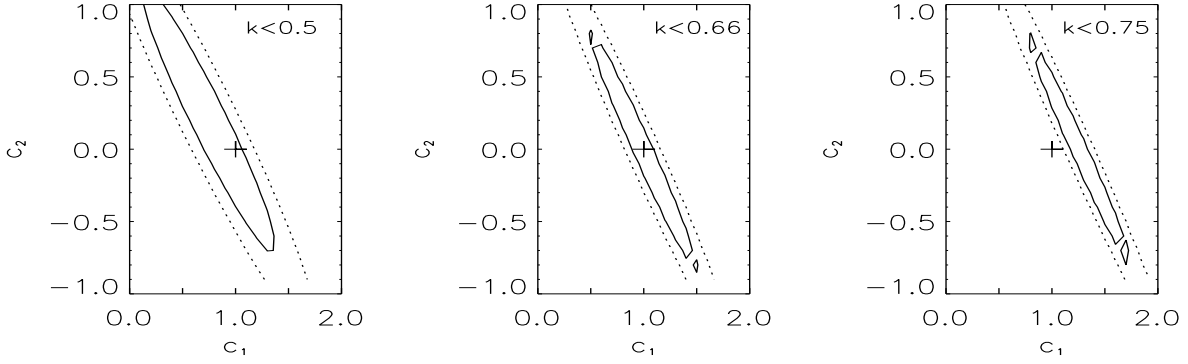


**Figure 3.** The real space joint likelihood for  $c_1$  and  $c_2$  as a function of the cutoff wavenumber employed, for a low-density CDM simulation with shape parameter  $\Gamma = 0.25$  and  $\sigma_8 = 1.06$ . The dotted and solid line contours contain 90 and 63 percent of the *a posteriori* probability  $P(c_1, c_2 | DATA)$  assuming uniform prior. The wavenumber corresponding to  $\Delta^2(k) = 1$  is  $k = 0.17$ . Second-order perturbation theory works well for the degenerate configuration up to  $k_{\text{short}} \simeq 0.66$ ; this corresponds to  $\chi^3 \simeq 100$ . This figure is relative to the final output ( $\sigma_8 = 1.06$ ) of the low- $\Omega_0$  simulation.

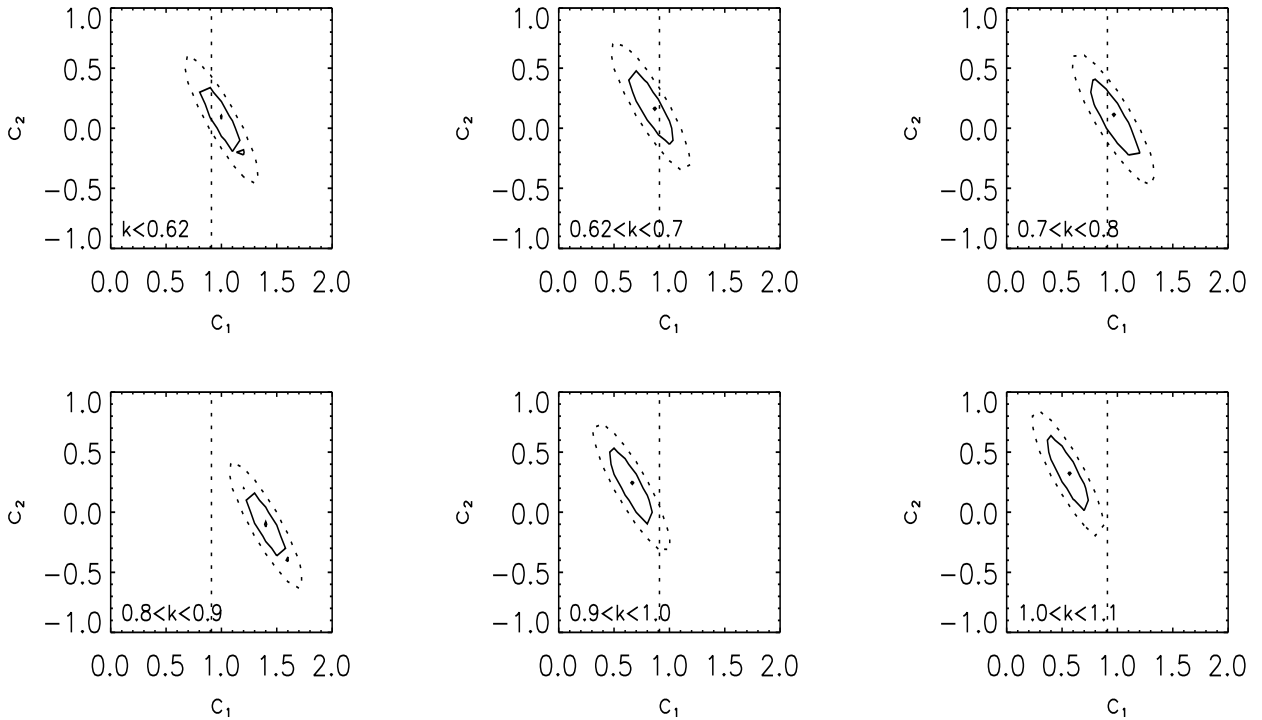


**Figure 4.** The real space joint likelihood for  $c_1$  and  $c_2$  for the biased catalogue. The dotted and solid line contours contain 90 and 63 percent of the *a posteriori* probability. In each panel  $k$ -vectors of the degenerate triangle configurations belong to a different shell in  $k$  space. For the equilateral configuration the  $k$ -vectors limits are  $0.3 < k < 0.5$  and for the degenerate the six shells are limited by: 0.62, 0.7, 0.8, 0.9, 1.0, 1.1. The first interval has been chosen in order to have about the same number of data as in the following interval and a signal of comparable strength. Second-order perturbation theory works well for the degenerate configuration up to  $k_{\text{short}} \simeq 0.8$  this corresponds to  $\chi^3 \simeq 100$ . The vertical dashed line shows the inverse of the effective bias of the power spectrum,  $\sqrt{P_g/P}$  at  $k = 0.8$ .

degenerate configuration  $0.5 < k_{\text{short}} < 0.8$ . The breakdown occurs where the normalized bispectrum  $\chi^3 = (2/\pi^2)k^6 B$  is  $\chi^3 \simeq 10$  for equilateral triangles and  $\chi^3 \simeq 100$  for degenerate triangles.

We also checked the behaviour of the 2OPT validity

range for a linearly biased catalogue. The catalogue has been created by applying equation (9) with  $b_1 = 1.4$ ,  $b_i = 0$  ( $i \geq 2$ ), to the density contrast field  $\delta(\vec{x})$  of the  $\Omega_0 = 1$ , unbiased simulation. In this case 2OPT breaks down for the same  $k$ -vectors values as in the unbiased case therefore where  $\chi^3$



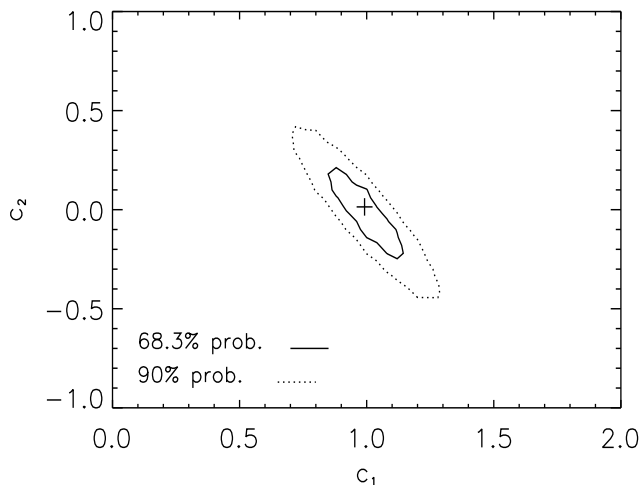


**Figure 5.** Joint likelihood of  $c_1 = 1/b_1$  and  $c_2 = b_2/b_1^2$ , for a CDM N-body simulation ( $\Omega_0 = 1$ ,  $\sigma_8 = 0.64$ ,  $\Gamma = 0.25$ , see text for further details), but in redshift space. Contours contain 68.3 and 90 per cent of the *a posteriori* probability  $P(c_1, c_2 | DATA)$  assuming uniform priors for  $c_1$  and  $c_2$ .

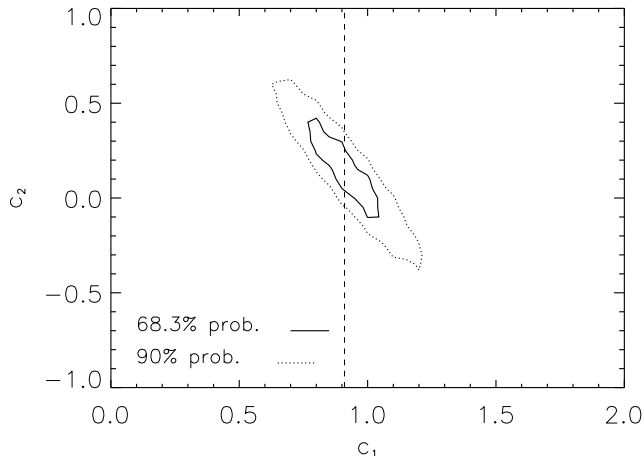


**Figure 6.** Joint likelihood of  $c_1 = 1/b_1$  and  $c_2 = b_2/b_1^2$ , for the real space N-body simulation (see text for details), but biased. The effective bias on scales where 2OPT holds is  $b_{\text{eff}}=1.1$  ( $1/b_{\text{eff}} = 0.91$ ) as indicated by the dashed line. Contours contain 68.3 and 90 per cent of the *a posteriori* probability.

is larger than the values previously determined. However, unless there is anti-bias, the  $\chi^3$  limit sets a conservative  $k$ -vector cutoff.

Finally we performed the likelihood analysis on the biased simulation with  $b_{\text{eff}} = 1.1$  in redshift space. Also in this more realistic case the analysis recovers the true value for the bias parameter within the errors (see Fig. 7). In this case the errors in the determination of the bias parameter are slightly bigger; this is due to the fact that the deter-

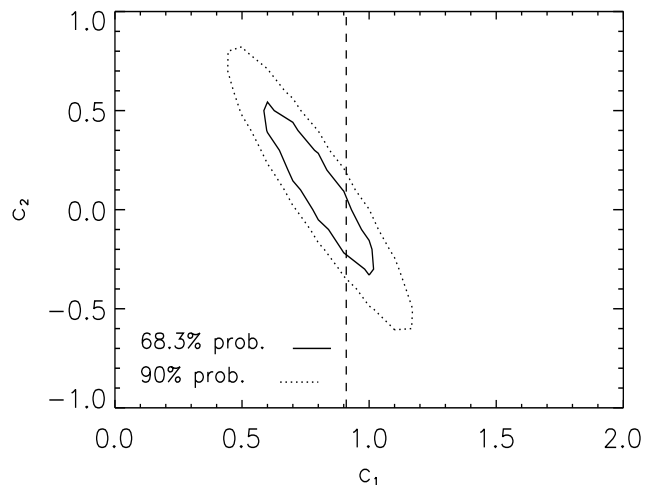


**Figure 7.** Joint likelihood of  $c_1 = 1/b_1$  and  $c_2 = b_2/b_1^2$ , for the biased simulation in redshift space. The effective bias on scales where 2OPT holds is  $b_{\text{eff}}=1.1$  ( $1/b_{\text{eff}} = 0.91$ ) as indicated by the dashed line. Contours contain 68.3 and 90 per cent of the *a posteriori* probability.

mination of the velocity dispersion is more noisy. In fact the adopted biasing scheme considerably increases the shot noise, and this propagates in a noisy determination of the velocity dispersion especially if the volume of the simulation is limited to a box of  $100 h^{-1}$  Mpc side. When applying the method to a real survey the volume available will be much larger, allowing a more precise determination of the velocity dispersion.

### 4.3 Results

For the flat Universe simulation in redshift space the joint likelihood for  $c_1$  and  $c_2$  for the limits on  $k$  set as described above, is shown in Fig. 5. The true value ( $c_1 = 1/b_1=1$ ,  $c_2 = b_2/b_1^2=0$ ) is remarkably recovered within the errors:  $1.02 \pm 0.15$  for  $c_1$  and  $-0.05 \pm 0.22$  for  $c_2$ .

The joint likelihood computed in the biased simulation for  $c_1$  and  $c_2$  for the limits on  $k$  set as in Section 4.2 is shown in Fig. 6 and Fig. 7, in real and redshift space respectively. Marginalising over  $c_2$ , the true value for the effective bias  $b_{\text{eff}} = 1.1$ ,  $c_{\text{eff}} = 1/b_{\text{eff}}$  is well recovered through  $c_1$ : we obtain  $c_1 = 0.93 \pm 0.15$ ,  $c_2 = 0.15 \pm 0.25$  for the real space case and  $c_1 = 0.90 \pm 0.22$ ,  $c_2 = 0.15 \pm 0.35$  for the redshift space case.

## 5 DISCUSSION

In Matarrese et al. (1997) we presented the first steps towards the goal of using the bispectrum to measure the linear bias parameter  $b$  from an ideal real-space galaxy distribution. The aim of this project is ultimately to combine measurements of  $b$  with estimates of  $\beta = \Omega_0^{0.6}/b$  from linear redshift distortion studies to get an estimate of the density parameter  $\Omega_0$ . In this paper, we have mainly tackled the

problem of redshift-space distortions, where peculiar velocities distort the three-dimensional map in redshift surveys. We have shown how the combination of second-order perturbation theory and an incoherent velocity dispersion model for virialised structures can successfully be used to estimate the bias parameter. This was not a trivial issue, since the signal for bias comes largely from the mildly non-linear regime, which is significantly affected by non-perturbative considerations.

We have also analyzed a biased simulation in real and redshift space: the bispectrum method successfully recovers the value for the bias parameter not only if we adopt a linear bias scheme, but also in a more realistic case where groups of dark matter particles are identified and each group counts as a galaxy.

To turn this into a practical application, one needs to be able to determine, in a consistent manner, where second-order perturbation theory breaks down. For the simulations we have analysed, the breakdown occurs when the real-space normalised bispectrum  $\chi^3$  (analogous to the quantity  $\Delta^2$  for the power spectrum) is  $\chi^3 \simeq 10$  for equilateral triangles, and 100 for degenerate triangles. This real-space quantity can be estimated, assuming, as we do, that  $\beta$  and the small-scale velocity dispersion  $\sigma$  can be estimated from the redshift-space power spectrum.

The practical limitations to the accuracy of the determination of  $b$  will be the size of the redshift survey, and the density of objects. Our suggestion for practical implementation is to divide the survey into a number of subsamples, within each of which we apply the distant-observer approximation and make an estimate of the bias parameter (marginalising over the second-order term  $c_2$ ). The size of the subsamples is determined by the non-linear scale,  $k \simeq 0.3$  if  $b \simeq 1$ , restricting the subsample sizes to about  $20 h^{-1}$  Mpc or larger. Since the signal comes from the weakly non-linear regime, the estimates may be assumed to be essentially uncorrelated. For the most distant subsamples, shot noise will prevent any useful information being obtained. This will restrict the depth to around  $z = 0.2$  for the forthcoming Anglo-Australian 2dF and SDSS. Nevertheless this gives a very large number (about 1800 and about 8000 respectively) of useful subvolumes (however, if the linear theory breaks down at  $k_{nl} \simeq 0.1$  the number of volume that one can obtain from the SDSS drops to about a thousand). Combining this with the estimated error on  $b$  from a single subvolume of about  $50 h^{-1}$  Mpc suggests that errors of about 5 per cent or less should be achievable. The statistical error on  $\beta$  from these surveys should be comparable or smaller (e.g. Ballinger et al. 1996; but see also Hatton & Cole 1998, Bromley et al. 1997), so the error on  $\Omega_0$  will be mainly determined by the error on  $b$  and should be around few percent.

## ACKNOWLEDGMENTS

LV acknowledges the support of TMR grant. Computations were made using STARLINK facilities. The simulations were obtained from the data bank of cosmological N-body simulations provided by the Hydra consortium (<http://coho.astro.uwo.ca/pub/data.html>) and produced using the Hydra N-body code (Couchman et al. 1995). We are particularly grateful to Peter Thomas for making

earlier epochs of the simulations available. AFH and LV thank the Dipartimento di Astronomia in Padova for hospitality. SM and LM thank the University of Edinburgh for hospitality. Thanks to Francesco Lucchin for useful discussions, and to John Peacock for comments on the manuscript.

## REFERENCES

- Ballinger W.E., Heavens A.F., Taylor A.N., 1995, MNRAS, 276, L59  
 Ballinger W.E., Peacock J.A., Heavens A.F., 1996, MNRAS, 282, 877  
 Bernardeau F., 1994, ApJ, 433, 1  
 Bersanelli M., Bouchet F.R., Griffin M., Lamarre J.M., Mandolesi N., Norgaard-Nielsen H.U., Pace O., Polny J., Puget J.L., Tauber J., Vittorio N., Volonté S., 1996, ESA D/SCI, 96, 3, COBRAS/SAMBA Report on the Phase A study  
 Bromley B.C., Warren M.S., Zurek W.H., 1997, ApJ, 475, 414  
 Catelan P., Moscardini L., 1994a, ApJ, 426, 14  
 Catelan P., Moscardini L., 1994b, ApJ, 436, 5  
 Cole S., Fisher K.B., Weinberg D.M., 1995, MNRAS, 275, 515  
 Colless M., 1996, in proceedings of the Heron Island Conference, <http://msowww.anu.edu.au/~heron/Colless/colless.html>  
 Couchman H.M.P., Thomas P.A., Pearce F.R., 1995, ApJ, 452, 797  
 Dekel A., Rees M.J., 1994, ApJ, 422, L1  
 Eisenstein D.J., 1997, preprint, astro-ph/9709054  
 Fan X., Bahcall N.A., Cen R., 1997, ApJ, 485, L53  
 Fisher K.B., 1995, ApJ, 448, 494  
 Fisher K.B., Scharf C.A., Lahav O., 1994, MNRAS, 266, 219  
 Fry J.N., 1994, Phys. Rev. Lett., 73, No. 2, 215  
 Gunn J.E., Weinberg D.H., 1995, Wide-field Spectroscopy and the distant Universe, proceedings of the 35th Herstmonceux workshop, Cambridge University press, Cambridge  
 Hamilton A.J.S., 1992, ApJ, 385, L5  
 Hamilton A.J.S., 1997, to appear in Proceedings Ringberg Workshop on Large-Scale Structure, Ringberg Castle, Germany September 1996, Kluwer Academic, Dordrecht (astro-ph/9708102)  
 Hatton S.J., Cole S., 1998, MNRAS, 296, 10  
 Heavens A.F., Taylor A.N., 1995, MNRAS, 275, 483  
 Hivon E., Bouchet F.R., Colombi S., Juszkiewicz R., 1995, A&A, 298, 643  
 Jungman G., Kamionkowski M., Kosowsky A., Spergel D.N., 1996, Phys. Rev. D54, 1332  
 Kaiser N., 1987, MNRAS, 227, 1  
 Mann R.J., Peacock J.A., Heavens A.F., 1997, MNRAS, 293, 209  
 Marzke R.O., Geller M.J., da Costa L.N., Huchra J.P., 1995, AJ, 110, 477  
 Matarrese S., Verde L., Heavens A.F., 1997, MNRAS, 290, 651 (MVH97)  
 Matsubara T., 1994, ApJ, 424, 30  
 Peacock J.A., 1992, in Martinez V., Portilla M., Saez D., eds, New insights into the Universe, Proc. Valencia summer school. Springer, Berlin, p.1  
 Peacock J.A., 1997, MNRAS, 284, 885  
 Peacock J.A., Dodds S.J., 1994, MNRAS, 267, 1020  
 Phillips S., 1994, MNRAS, 269, 1077  
 Scoccimarro R., Colombi S., Fry J. N., Frieman J. A., Hivon E., Melott A., 1998, ApJ, 496, 586  
 Strauss M.A., Willick J.A., 1995, Phys. Rep., 261, 271  
 Zurek W.H., Quinn P.J., Salmon J.K., Warren M.S., 1994, ApJ, 431, 559

## APPENDIX A: EXPRESSION FOR THE N-POINT GALAXY SPECTRA IN REDSHIFT SPACE

Following the mathematical method outlined in Section 3 of MVH97 it is possible to calculate the galaxy N-point spectra in redshift space. The expression for the N-point spectra includes the large scale effect to second order in perturbation theory (equation 11) and the small scale effect due to the velocity dispersion of the galaxies with velocity distribution modelled by an exponential (equation 5).

The expression for the external source  $\mathcal{J}_k^d$  is still given by:

$$\mathcal{J}_k^d(\vec{x}) = -iN \left\{ \exp \left[ \frac{i}{N} \sum_{m=1}^N s_m e^{-i\vec{k}_m \cdot \vec{x}} \widetilde{W}(\vec{k}_m) \right] - 1 \right\}, \quad (\text{A1})$$

but now the Fourier transform of the smoothing function ( $\widetilde{W}$ ) includes the effect of the filter:

$$\widetilde{W}(\vec{k}_m) = \frac{1}{\sqrt{1 + k_m^2 \sigma^2 \mu^2 / 2}}. \quad (\text{A2})$$

The Ansatz for the generating functional is still the same: assuming Gaussian initial conditions and allowing for a quasi-linear evolution in 2OPT approximation all the irreducible correlation functions  $\xi_{\text{conn.}}^n$  of order  $n > 3$  are negligible. But the difference is that in the expression for the generating functional

$$\begin{aligned} \mathcal{Z}[\mathcal{J}_k] = & \exp \left[ i \int d^3x \mathcal{J}_k(\vec{x}) - \frac{1}{2} \int d^3x d^3x' \mathcal{J}_k(\vec{x}) \mathcal{J}_k(\vec{x}') \xi_{\text{conn.}}^{(2)\text{red}}(\vec{x}, \vec{x}') \right. \\ & \left. - \frac{i}{6} \int d^3x d^3x' d^3x'' \mathcal{J}_k(\vec{x}) \mathcal{J}_k(\vec{x}') \mathcal{J}_k(\vec{x}'') \xi_{\text{conn.}}^{(3)\text{red}}(\vec{x}, \vec{x}', \vec{x}'') \right], \end{aligned} \quad (\text{A3})$$

now  $\xi_{\text{conn.}}^{(2)\text{red}}$  and  $\xi_{\text{conn.}}^{(3)\text{red}}$  includes the redshift space effects that yield equations (11) to (16) (Heavens et al., in preparation).

With these modifications the generating functional approach outlined in MVH97 allows calculation of N-point spectra and their covariance properties directly in redshift-space taking also into account non-linearities to second order in perturbation theory. The advantages are manifold since non-linearities affect the statistics of the density field even on quite large scales and, at the same time, there is the necessity to push the analysis to smaller scales to improve the statistics.

The general prescription turns out to be that for a given configuration of  $\{\vec{k}_i\}_{i=1\dots N}$  the N-point spectrum  $\langle \delta_{\vec{k}_1} \dots \delta_{\vec{k}_N} \rangle$  is first calculated consistently with 2OPT for the density field and the redshift distortion, and then has to be ‘filtered’ with N damping factors as in equation (5) each one relative to one  $\delta_{\vec{k}_i}$ .

The galaxy bispectrum in redshift space for a given triangle configuration is a special case where  $N = 3$  and it is given in equation (19).

## APPENDIX B: CONSTRAINTS ON THE NUMBER OF SUBSAMPLES

In MVH97 we showed that the signal to noise of the bias estimate can be improved by splitting the volume in subsamples. This is certainly true if the errors on the power

spectra are negligible, but it may not be true if the subsamples are too small and the spectra become noisy or if the real space power reconstruction procedure yields the power spectrum with uncertainties.

However it is possible to calculate the entity of the error on the bias parameter due to uncertainty in the power spectrum as follows. We ignore shot noise for simplicity and we refer to equilateral triangles. Since the likelihood adds information inversely weighted by variance, the error on  $c_1$   $\sigma_{c_1}$  is given by

$$\frac{1}{\sigma_{c_1}^2} = \sum_{\text{shells}} \frac{1}{\sigma_{c_1}^2(\text{shell})}, \quad (\text{B1})$$

$\sigma_{c_1}(\text{shell})$  being the contribution to the error on  $c_1$  from a thin shell of radius  $k$  in  $k$ -space.

This can be expressed in terms of the error on the power spectrum. Let  $P(k)$  be the average power in the shell in  $k$ -space;  $P(k)$  is constant in the shell and has a variance  $\sigma_{P(k)}^2$ . Therefore

$$\sigma_{c_1}^2(\text{shell}) = \left( \frac{2 \sum_{\nu} P(k)}{\sum_{\nu} P(k)} \right)^2 \sigma_{P(k)}^2 = \frac{4\sigma_{P(k)}^2}{P(k)^2}, \quad (\text{B2})$$

where  $\nu$  labels the triangles.

Summing the contributions from all the shells,

$$\sigma_{c_1}^2 = \frac{1}{\sum_{\text{shells}} \frac{P^2}{4\sigma_P^2}}, \quad (\text{B3})$$

and passing to the continuum limit, under the hypothesis that  $P$  is affected only by statistical error, we obtain

$$\sigma_{c_1}^2 = \frac{4}{\frac{V4\pi}{2(2\pi)^3} \int_{k_{\min}}^{k_{\max}} k^2 dk} = \frac{\gamma^2}{V}, \quad (\text{B4})$$

where  $V$  is the volume of the sample in units of  $h^{-3}$  Mpc<sup>3</sup>. If  $k_{\max}$  is the same as in real space ( $k_{\max}$  previously found was 0.55), we have  $\sigma_{c_1} \simeq 53/\sqrt{V}$ . As we have seen, the redshift-space  $k_{\max}$  can be pushed towards higher  $k$ , reducing the error on  $c_1$ : if  $k_{\max} = 0.85$  as we found here, then  $\sigma_{c_1} \simeq 28/\sqrt{V}$ .

Therefore splitting the volume in  $M$  subvolumes is still effective if

$$\frac{\sigma_{c_1}^2(B)}{M} \gg \frac{\gamma M}{V_{SV}} = \frac{\gamma}{V_{\text{tot}}}, \quad (\text{B5})$$

where  $\sigma_{c_1}(B)$  is the error on  $c_1$  due to the variance in the bispectrum,  $V_{SV} = V_{\text{tot}}/M$  is the volume of the subsamples. This is a constraint on the number of subsample to make, once the properties of the selection function of the survey and the range of validity of 2OPT are known.

As long as the errors on the reconstructed real-space power spectrum are of the same order of its statistical errors, and if still, as we found in the simulation,  $\sigma_{c_1}^2(B) \simeq 0.5$  and the optimal size for the subvolumes is  $\simeq 20h^{-1}$  Mpc (MVH97), then the use of the subvolumes is still effective both for SDSS and 2dF surveys. Any additional uncertainty on the power spectrum will alter the right-hand side of equation (B5) placing a stronger constraint on the number of subvolumes and/or on their size.